From genomic decay to functional advantage: Trait-based evidence for long-term host residency of a next-generation coral probiotic

Mei Xie[1], Congjuan Xu[1], Nan Xiang[1], Tianhua Liao[1], Xing Liu[1], Zhiqi Liu[2], Xiaoyuan Feng[1], Qian He[1], Zizhen Liang[2], Weiqi Wang[1], Yifan Dai[2], Lili Yan[2], Claudia Pogoreutz[3], Lena Barra[4], Shannon Wing Ngor Au[2], Liwen Jiang[2], Christian R. Voolstra[5], Haiwei Luo[1, 6, 7*]

[1]Simon F. S. Li Marine Science Laboratory, School of Life Sciences, The Chinese University of Hong Kong, Shatin, Hong Kong SAR
[2]School of Life Sciences, The Chinese University of Hong Kong, Shatin, Hong Kong SAR
[3]PSL Université Paris: EPHE-UPVD-CNRS, UAR 3278 CRIOBE, Université de Perpignan, Perpignan Cedex, France
[4]Fachbereich Chemie, Universität Konstanz, Universitätsstraße 10, 78464 Konstanz, Deutschland
[5]Department of Biology, University of Konstanz, Konstanz, Germany
[6]State Key Laboratory of Agrobiotechnology, The Chinese University of Hong Kong, Shatin, Hong Kong SAR
[7]Institute of Environment, Energy and Sustainability, The Chinese University of Hong Kong, Shatin, Hong Kong SAR

***Corresponding author:**
Haiwei Luo
School of Life Sciences, The Chinese University of Hong Kong
Shatin, Hong Kong SAR
Phone: (+852) 3943-6121
Fax: (+852) 2603-5646
E-mail: haiweiluo@cuhk.edu.hk

Running title: Probiotic traits for coral residency

Key words: Coral probiotics, *Ruegeria*, symbiosis, next-generation probiotics

Abstract

A key bottleneck in microbiome engineering is ensuring the long-term host association of introduced microbes. Selecting probiotic candidates based on evolutionary genomic decay signatures of host dependency offers a potential solution. The *Ruegeria* strain B4 of the population MC10, identified by such signatures, has shown persistent colonization in corals. To understand the putative mechanisms behind this, we characterized its functional profile using an integrated multi-omics approach, comparing it to non-candidate *Ruegeria* strains isolated from the same coral colony and compartment (mucus). This controlled for host genotype and microenvironment, both of which influence colonization outcomes. We show that MC10's genome is uniquely enriched for host-interaction functions, such as siderophore-mediated iron acquisition and exopolysaccharide biosynthesis, which were confirmed phenotypically by enhanced siderophore production and biofilm formation. Subsequent proteomic analysis showed that the MC10-B4 proteome underwent a "motility-to-sessility" reprogramming upon exposure to host metabolites, a response distinct from its non-candidate sympatric relatives. Our findings suggest an evolutionary shift toward host dependency, marked by genomic decay on one hand and compensated by the gain and expression of functions that enable stable colonization on the other. MC10's functional profile, particularly its sensitivity to oxidative stress, would likely have excluded it from conventional probiotic screens that prioritize robust in vitro performance. This validates an evolution-guided approach that prioritizes innate colonization potential over pre-defined *in vitro* functionalities, informing the rational design of next-generation probiotics.

Introduction

Coral reefs are foundational marine ecosystems experiencing severe global decline, largely due to mass bleaching events triggered by climate change (Hughes et al., 2017; Reimer et al., 2024). The breakdown of the symbiotic relationship between corals and their photosynthetic dinoflagellates (Symbiodiniaceae) leads to host starvation and mortality (Rädecker et al., 2021), creating an urgent need for interventions that can enhance resilience (Hughes et al., 2017; Voolstra et al., 2021).

The targeted application of beneficial microorganisms, or probiotics, has emerged as a promising strategy to mitigate coral stress (Peixoto et al., 2021). Laboratory and mesocosm studies have demonstrated that probiotic inoculations can improve thermal tolerance and disease resistance in corals (Li et al., 2023; Santoro et al., 2021). However, a critical bottleneck constrains the scalable application of this approach across conservation, aquaculture, and agriculture: the uncertain long-term residency of administered probiotics within the host holobiont (Čaušević et al., 2024; Peixoto et al., 2021). This challenge of transient colonization is universal; it not only limits the duration of beneficial effects but also raises the fundamental question of whether observed improvements stem from short-term nutritional supplementation or the establishment of a stable, beneficial symbiosis.

Conventional probiotic selection often focuses on screening for predefined beneficial traits in vitro (Santoro et al., 2021). To address the colonization bottleneck, we recently proposed a novel framework for selecting what we term next-generation probiotics (NGPs), which are chosen based on evolutionary genomic signatures indicative of an irreversible transition toward host dependency (Xie et al., 2025). The core, previously untested hypothesis was that bacterial lineages exhibiting genomic hallmarks of this transition, such as insertion sequence (IS) expansion and prevalent pseudogenization of core metabolic genes, which are parallel to those seen in terrestrial symbiotic models like *Sodalis glossinidius* (Clay, 2014), would be predisposed for stable colonization in a probiotic context. This evolution-guided approach inverts the conventional pipeline by first predicting persistence and then empirically testing for beneficial effects.

The practical application of this evolution-guided framework led to the identification of the *Ruegeria* population MC10 as an NGP candidate from a collection of 1,212 coral-associated bacterial isolates (Xie et al., 2025). Strains from this population, including MC10-B4, were selected based on genomic decay signatures indicative of a trajectory towards host dependency, such as insertion sequence expansion and pseudogenization of essential pathways like the tricarboxylic acid (TCA) cycle. This in turn suggested an *a priori* potential for long-term residency to compensate for metabolic deficiencies through host-derived metabolites. The candidate was then advanced to an independent screening step using a standardized acute heat stress assay on a model cnidarian, *Exaiptasia diaphana* (Dörr et al., 2023). This assay confirmed that MC10-B4 inoculation was associated with a significant increase in host thermal tolerance, indicating a potential functional benefit (Xie et al., 2025). Based on its predicted persistence and an observed functional benefit in a controlled assay, the strain was advanced to a field trial. There, a one-month, twice-weekly nursery inoculation of the coral *Acropora pruinosa* with MC10-B4 enabled the strain to establish and be retained in coral tissues for the entire eight-month monitoring period post-outplanting. This sustained retention included persistence through a natural bleaching event, during which inoculated

corals showed reduced visual bleaching and better maintenance of photosynthetic efficiency compared to uninoculated, placebo (autoclaved filtered seawater)-treated controls (Xie et al., 2025).

A critical knowledge gap remained following the proof-of-concept demonstration for the *Ruegeria* MC10 NGP. While the sustained retention of MC10 and its association with coral resilience were established, the genomic and functional mechanisms underpinning its successful colonization and potential beneficial role remained unexplored. Understanding these mechanisms is vital to provide mechanistic support for how the evolutionary selection framework achieves its success and to build a generalizable, trait-based understanding of the determinants of stable colonization. Such insights are crucial for informing the rational design of future probiotic interventions across diverse host systems.

In this study, we use a multi-omics approach primarily to investigate the mechanistic basis of *Ruegeria* MC10's persistent host association. We test the hypothesis that its evolutionary trajectory toward host dependency is underpinned by a suite of traits conducive to stable colonization. Secondarily, we contextualize these colonization mechanisms with its previously established probiotic function, i.e., increased host thermal resilience. Comparative genomics with *Ruegeria* isolates at large identified MC10-specific genetic features conducive to a host-associated lifestyle. These features were then contextualized with phenotypic assays and proteomic profiling of MC10's response to coral metabolites. Crucially, MC10-B4 was compared against two sympatric *Ruegeria* strains (MC0-A5 and MC15-BG7) isolated from the same coral colony and compartment (mucus). This analytical framework controlled for host genotype, micro-environment, and sampling time to identify the functional traits linked to MC10's distinct evolutionary trajectory. Our analyses provide insight into how signatures of genomic decay suggestive of a trajectory towards host dependency, on the one hand, align with the acquisition of functional traits conducive to host beneficial effects on the other hand, informing the future design of probiotic interventions.

Materials and Methods

All detailed methodologies are provided in the Supplementary Materials. Briefly, a total of 419 *Ruegeria* strains were cultured from five coral species, *Acropora* cf. *samoensis*, *A. solitaryensis*, *Favites pentagona*, *Platygyra acuta*, and *Oulastrea crispata*, which were sampled across nine reef sites in Hong Kong. To elucidate the mechanisms underlying the persistent colonization of the candidate coral probiotic *Ruegeria* population MC10, we employed an integrated multi-omics and phenotypic profiling approach. We first conducted comparative genomic analyses of MC10 against other co-occurring *Ruegeria* strains to identify specific genomic features. A total of 34 strains (15 from MC10, two from its sister MC46, and one each from 17 other MCs) were sequenced using Oxford Nanopore Technologies (ONT) to generate closed or near-closed genomes. These were supplemented with 419 draft genomes (including those of the above 34 strains) from Illumina next-generation sequencing (NGS) and 26 genomes from public databases, resulting in a final dataset of 445 *Ruegeria* genomes. Orthologous gene families were identified with OrthoFinder v2.5.1 (Emms et al., 2015). Prophage regions were predicted using the "What the Phage" workflow (Marquet et al., 2022) and refined with PHASTEST v1.0.0 (Wishart et al., 2023). Toxin-antitoxin systems were predicted using antiSMASH v7.0 (Blin et al., 2023),

and CRISPR-Cas systems were identified with CasFinder v3.1.0, a specialized module implemented in the Macsyfinder v2.1.1 framework (Abby et al., 2014). DMSP degradation-related genes were annotated using the DiTing database v0.95 (Xue et al., 2021). Gene distribution patterns were quantified by determining the presence or absence of each KEGG Ortholog (KO) across all analyzed genomes. MC10-specific traits were identified by comparing gene presence and absence against non-MC10 lineages, while shared novel probiotic traits were uncovered by benchmarking all *Ruegeria* annotated genes against a curated dataset to reveal potentially probiotic traits that were not reported previously.

We then performed targeted phenotypic assays, comparing MC10-B4 (a representative strain from MC10) to two non-candidate, sympatric strains (i.e., MC0-A5 and MC15-BG7, selected from the populations MC0 and MC15 respectively), which were isolated from the same coral colony and mucus compartment as MC10-B4 to control for host genotype and microenvironment. The model pelagic bacterium *R. pomeroyi* DSS-3 was included to provide a broader phylogenetic context. A comprehensive suite of assays was employed: bacterial intracellular inclusions was examined via transmission electron microscopy; motility was assessed through swimming (0.18% agar), swarming (0.75% agar), and twitching assays, alongside sedimentation in static cultures. Biofilm production was quantified using a crystal violet-based microtiter plate assay; siderophore synthesis was detected via the Chrome Azurol S (CAS) assay (Louden et al., 2011), indicated by a color change from blue to orange; vitamin auxotrophy assays were performed by cultivating the four *Ruegeria* strains in a marine basal medium lacking either vitamin B_7 (biotin) or B_{12} (cobalamin). Furthermore, we tested their sensitivity to a series of environmental and chemical challenges: oxidative stress was assessed by spotting serial dilutions onto H_2O_2-supplemented agar and a liquid kill assay to quantify bacterial survival; catalase activity was determined visually by the production of oxygen bubbles upon exposure to 3% H_2O_2; antibiotic susceptibility was profiled against eight antibiotics using the standard disk diffusion method; and growth sensitivity to a range of pH (5.0-8.0) was recorded after four-day incubation.

For a proteomic analysis, bacterial cultures pre-cultured to exponential phase were exposed to coral tissue extract or autoclaved filtered seawater control for 4 hours. After treatment, cells were lysed by boiling in the SDS buffer, and proteins were separated via SDS-PAGE. In-gel digestion was carried out, including reduction with dithiothreitol (DTT), alkylation with iodoacetamide (IAA), and overnight digestion with sequencing-grade trypsin. The resulting peptides were extracted, desalted using C18 spin columns, and analyzed by liquid chromatography-tandem mass spectrometry (LC-MS/MS) on an Orbitrap Fusion Lumos Tribrid mass spectrometer. For precise identification and quantification, raw spectra were processed with Proteome Discoverer v3.1.0 (Orsburn, 2021) and matched against custom, strain-specific protein databases generated from their annotated genomes. A label-free quantification (LFQ) workflow incorporating retention time alignment and feature mapping was employed to normalize spectral intensities and determine relative protein abundance. Beta diversity was evaluated via PCoA (based on Bray-Curtis). Differential expression analysis was performed using the limma algorithm, identifying significantly different expressed proteins with a false discovery rate (FDR) < 0.05 and an absolute log2 fold change > 0.5.

Results

Comparative genomics reveals *Ruegeria* MC10's unique repertoire of host-adaptation genes

To investigate the genetic features underlying *Ruegeria* MC10's host-associated lifestyle, we first characterized its genomic architecture and gene content. From a collection of 419 *Ruegeria* isolates sourced from five coral species across nine Hong Kong reef sites, we generated 35 high-quality closed genomes. Population boundaries were delineated using PopCOGenT, a tool that identifies genetically cohesive groups based on barriers to homologous recombination, which resolved 116 distinct *Ruegeria* populations designated as Main Clusters (MCs; Fig. S1). This population-level resolution enabled targeted comparisons between MC10 and other lineages, with a specific focus on sympatric controls MC0-A5 and MC15-BG7. These control strains were isolated from the exact same *Oulastrea crispata* colony and compartment (mucus) as MC10-B4, thereby controlling for variation attributable to host genotype, micro-environment, and sampling time.

Analysis of the closed genomes revealed that the MC10 population possesses a larger chromosome (4.52 ± 0.02 Mb, except that MC10-AC11 has a less complete chromosome which is 3.51 Mb) compared to other *Ruegeria* MCs, which typically range from 3.22 to 4.04 Mb (Fig. 1B). A defining architectural feature was the integration of plasmid-derived sequences into the chromosome, a phenomenon not observed in other lineages (Fig. 1A). Furthermore, the extrachromosomal plasmids carried by MC10 isolates (ranging from two to three per genome) were exclusively associated with this population and were notably smaller (0.133 to 0.443 Mb) than the large, often >1 Mb, plasmids found in other MCs. MC10 genomes were also enriched with integrated prophage regions, harboring four to five intact prophages (e.g., prophages in MC10-B4 labeled in Dataset S1) spanning 120-160 Kbp per genome, with a cumulative size markedly higher than the 0-3 prophages (totalling <70 Kbp) typical of other lineages, except for MC45-AM7, which had a comparable profile (Fig. 1C, Fig. S2). This distinct genomic architecture, characterized by chromosome expansion, plasmid integration, and a high prophage burden, is consistent with patterns observed in early-stage endosymbionts undergoing genomic reorganization. Critically, these architectural signatures are conserved across all MC10 isolates, indicating they originated in the population's last common ancestor.

We next sought to contextualize the genetic repertoire of *Ruegeria* MC10 within the broader diversity of coral-associated *Ruegeria*. Clustering of the ~10,400 gene families from the 35 closed genomes (4119 ± 43 for each) revealed three broad genomic blocks: a core set of ~3,200 gene families conserved across all populations, ~5,700 gene families that were sparsely distributed in other *Ruegeria*, and ~1,500 gene families that were distinctly prevalent in the MC10 population (Fig. 1A). This structure indicates that approximately 31% of MC10's genomic regions are distinct and rarely found in other coral-associated *Ruegeria*, underscoring its divergent evolutionary path. Analysis of these MC10-enriched genes (all genes discussed in this section can be found in Dataset S1) revealed a uniquely coordinated oxidative stress defense system (Fig. 2A). This includes a core enzymatic arsenal for neutralizing reactive oxygen species (ROS), with universal possession of catalases (*katE*, *katG*) and specific peroxidases (cytochrome c peroxidase, glutathione peroxidase) that are significantly more prevalent in MC10 than in other *Ruegeria* populations. For instance, *katE*

is universal in MC10 (15/15) but found in only 109 of 404 non-MC10 isolates, and glutathione peroxidase is present in all MC10 isolates versus 270 non-MC10 isolates. Furthermore, MC10 possesses a complete Class Ib ribonucleotide reductase (RNR) operon (*nrdHIEF*), essential for maintaining deoxynucleotide (dNTP) pools for DNA synthesis and repair during oxidative stress (Roca et al., 2008), which was present in 14/15 MC10 genomes but largely absent (36/404) in the other *Ruegeria* isolates. Similarly, the cytochrome bd oxidase gene cluster (*cydABCD*), which supports respiration under low-oxygen conditions and provides protection against oxidative and nitrosative stress through its catalase activity (Cai et al., 2021; Giuffrè et al., 2014), was exclusively identified in MC10 (15/15 MC10 vs. 83/404 for *cydAB* and 0/404 for *cydCD* in other isolates). The universal stress protein gene *uspE*, which confers broad-spectrum protection against environmental challenges, was also a hallmark of the MC10 population (15/15 MC10, 2/404 other isolates). This distinctive genetic arsenal equips MC10 with robust mechanisms to manage stressors prevalent in a host-associated environment.

A suite of genes implicated in host interaction and biofilm formation was also distinctly prevalent in MC10. This included a diverse repertoire of glycosyltransferases (GTs) from families GT2 (involved in the transfer of sugars to polysaccharides and lipids for biofilm matrix and capsule production, 15/15 MC10 vs. 10/404 other isolates), GT25 (catalyzing sugar transfer in lipopolysaccharide biosynthesis, 8/15 MC10 vs. 0/404 other isolates), and GT51 (peptidoglycan glycosyltransferase for cell wall construction, 13/15 MC10 vs. 0/404 other isolates), alongside a defining cluster of genes for exopolysaccharide (EPS) production and secretion (*exoL*, *exoX*, *exoU*, *exoO*, *exoQ*, *exoP*, *TC.PST*, 15/15 MC10 vs. 12/404 other isolates) and cell envelope modification (*rfbFGH* for CDP-6-deoxyhexoses biosynthesis, 15/15 vs. 129/404; *glf* for UDP-galactopyranose mutase, 15/15 vs. 89/404; *gnu* for glycoside hydrolase, 15/15 vs. 3/404; *ompV* for membrane transporter, 15/15 vs. 62/404) (Fig. 2B). Furthermore, MC10 uniquely harbors genes for specialized sugar metabolism, including *rhaM* and *rhmD* for rhamnose metabolism, *fucD* for fucose metabolism, and *bshB1* for sugar deacetylation. These features collectively suggest an enhanced capacity for biofilm matrix production, cell surface modification, and carbohydrate utilization, traits that are often associated with initiating stable host associations (Ravichandran et al., 2025; Skorupska et al., 2006).

A critical genomic innovation of MC10 is its distinct capacity for high-affinity iron acquisition, based on the gene families present. In the analysis, MC10 was distinguished by the presence of a complete gene cluster for the biosynthesis of the siderophore, including the synthetase genes *entA*, *entE*, *entC*, *entF*, *mbtH*, *entS*, and *entD*, which were highly specific to MC10 (15/15 MC10 vs. 2/404 other isolates) (Fig. 2A). This biosynthetic capability is complemented by the characteristic encoding of several outer membrane receptor proteins for iron acquisition: TC.FEV.OM (an iron complex outer membrane receptor protein, 14/15 vs. 107/404), TC.FEV.OM2 (a receptor for ferrienterochelin and colicins, 15/15 vs. 2/404), and TC.FEV.OM3 (a receptor for hemoglobin, transferrin, and lactoferrin, 15/15 vs. 74/404). This comprehensive siderophore system provides a powerful mechanism for scavenging iron in the iron-limited host environment (Dellisanti et al., 2024; Hood et al., 2012).

Finally, MC10's genome is markedly enriched with specialized defense systems that may contribute to its persistence and ecological safety. It characteristically harbors numerous

toxin-antitoxin (TA) systems, including *doc-phd* (15/15 MC10 vs. 0/404 other isolates), *hipA-hipB* (14/15 vs. 54/404), *ccdB-ccdA* (15/15 vs. 177/404), (Fig. 2A). The functions of these toxins are diverse: *doc* targets the protein synthesis machinery, *ccdB* targets DNA gyrase, *hipA* inactivates glutamyl-tRNA synthetase (*GltX*), and *fitB* acts as an RNA-cleaving nuclease. Notably, the MC10-B4 strain also possesses a set of genes for CRISPR-associated (Cas) genes, including *cas1* (14/15 vs. 2/404), Csa3 (15/15 vs. 17/404), and *cas9* (12/15 vs. 2/404) (Fig. 2A), indicating a potential capacity for adaptive immunity against phage predation. This defensive repertoire is supplemented by the hallmark presence of a type I restriction-modification system (*hsdRSM*), exonuclease SbcB, and restriction enzyme Mrr. The abundance of these defense genes equips MC10 with robust mechanisms to maintain genomic integrity against mobile genetic elements and phage attacks, potentially enhancing its stability as a probiotic inoculant (Barrangou et al., 2014; Getz et al., 2024).

Phenotypic traits of *Ruegeria* MC10 are consistent with genomic predictions of a host-adapted symbiont

To determine whether the genomic features of *Ruegeria* MC10 manifest as realized cellular traits, we conducted a series of phenotypic assays under controlled laboratory conditions. For a rigorous assessment, we focused on three strains, MC10-B4, MC0-A5, and MC15-BG7 that were isolated from the same *Oulastrea crispata* coral colony and compartment (mucus), thereby controlling for their ecological origin. The free-living, pelagic model strain *Ruegeria pomeroyi* DSS-3 was included as a benchmark control.

Transmission electron microscopy (TEM) revealed strain-specific differences in intracellular inclusions; bright white storage granules, likely polyhydroxyalkanoates (PHAs), and light grey putative lipid droplets were prominent in DSS-3 and MC0-A5 but were significantly reduced in MC10-B4 and absent in MC15-BG7 (Fig. 3A). The reduced PHA reserves in MC10-B4 may reflect a diminished need for carbon storage or a reduced capacity for osmoprotection, consistent with a potential shift from a free-living to a more stable, host-associated lifestyle where resources are more constant and osmotic stress is buffered by the host (Sedlacek et al., 2019).

As motility is a key trait for environmental bacteria to locate and colonize host tissues (Ganesan et al., 2022), we assessed this phenotype. Swim plate assays in 0.18% soft agar showed that strain MC10-B4 displayed an intermediate motility phenotype, confirmed by sedimentation assays (Fig. 3B). Under the same conditions, strain MC0-A5 was highly motile, while strains DSS-3 and MC15-BG7 showed minimal movement. This confirms that MC10-B4 is motile, expressing a functional trait consistent with a host-colonizing symbiont. No swarming or twitching motility was observed for any strain (Fig. 3C).

We next examined the capacity for biofilm formation, a trait critical for transitioning to a stable, surface-associated lifestyle (Rumbaugh & Sauer 2020). MC10-B4 developed substantially more robust biofilms on the surfaces of microtiter plates compared to MC0-A5 and MC15-BG7 (Fig. 3D). As expected, the free-living model strain DSS-3 did not form a detectable biofilm under these conditions (Fig. 3D). This pronounced phenotypic difference is strongly consistent with MC10's unique genotypic endowment, which is enriched with genes for EPS production and a diverse repertoire of glycosyltransferases (GT; Fig. 2B), suggesting an increased capacity to produce an extracellular matrix required for stable host

attachment (Nadell et al., 2015).

Genomic predictions related to nutrient acquisition were further phenotypically tested. The prediction that MC10-B4 possesses a distinct siderophore biosynthesis cluster was supported by the chrome azurol S (CAS) assay, where it was the only strain among those tested that produced detectable siderophores (Fig. 3E), suggesting a mechanism for scavenging iron in the potentially iron-limited host environment. Furthermore, genomic analysis had suggested potential auxotrophy for vitamin B_7 (biotin) and B_{12} (cobalamin). However, growth assays revealed that for all four strains, growth patterns were nearly identical across treatments with full vitamin supplementation, no vitamins, no vitamin B_{12}, or no vitamin B_7 (Fig. 3F). Although the growth rate was generally slightly lower in the complete absence of vitamins, one-way ANOVA showed that the final biomass yield was not significantly changed in the vast majority of cases. The only exceptions were the significant differences observed between +Vfull and -Vita12 in strain BG7 ($P = 0.0169$) and between -Vita12 and -Vita7 in strain DSS-3 ($P = 0.0411$). All other pairwise comparisons were non-significant ($P > 0.05$). This indicates that, under the tested *in vitro* conditions, all strains, including MC10-B4, can synthesize these vitamins *de novo*, revealing a disparity between the genomic predictions of auxotrophy and the phenotypic outcomes in a nutrient-replete medium. This suggests a potential functional rescue despite pseudogenization, possibly via mechanisms such as ribosomal frameshifting or codon redefinition that allow translation of disrupted genes (Feng et al., 2022; Xie et al., 2025).

We also assessed traits that could influence MC10-B4's ability to survive independently outside a host environment. Phenotypic assays showed that MC10-B4 does not exhibit elevated resistance to a broad spectrum of antibiotics, including tetracycline (TE 30), neomycin (N 30), nitrofurantoin (F 100), cefuroxime (CFR 30), gentamicin (CN 10), erythromycin (E 15), vancomycin (VA 30), and chloramphenicol (C 30). It was in fact more susceptible to nitrofurantoin (F 100), erythromycin (E 15), and vancomycin (VA 30) than MC0-A5 or both MC0-A5 and MC15-BG7 (Fig. S3). Furthermore, MC10-B4 showed no exceptional tolerance to extreme pH, failing to grow at pH 5 or 6 while growing robustly at pH 7 and 8, a profile identical to MC0-A5 and MC15-BG7 (Dataset S2). A critical finding emerged from assays evaluating tolerance to oxidative stress. Contrary to an initial hypothesis that a host-adapted symbiont might possess the machinery to counter reactive oxygen species to enhance resilience, MC10-B4 was uniquely sensitive to hydrogen peroxide (H_2O_2) compared to the other strains (Fig. 3G, S4). This phenotypic sensitivity was consistent with a simple catalase slide test, which revealed that both MC10-B4 and MC0-A5 lacked detectable catalase activity, whereas MC15-BG7 tested positive. Notably, strain DSS-3 also produced the enzyme but at a lower level (Fig. S4). This finding is significant for interpreting the mechanism and niche of MC10's probiotic effect.

This inherent sensitivity to both oxidative and low pH stress informs its possible *in hospite* colonization site. The microenvironment immediately surrounding Symbiodiniaceae cells is characterized by a highly acidic pH (~4), maintained by host V-ATPase activity (Barott et al., 2015), and it might be also a site of elevated H_2O_2 production originating from algal photosynthesis (Lesser, 2006). Our phenotypic data show that MC10-B4 is poorly suited to thrive under these combined conditions. This is consistent with our FISH imaging, which showed that most MC10 cells are not in close proximity to Symbiodiniaceae cells in

hospite (Xie et al., 2025). Together, this evidence suggests that MC10-B4 is less likely to use the symbiosome microenvironment or symbiotic coral cells as its primary niche and instead colonizes other host compartments.

Proteomic profiling under host metabolite exposure reveals a colonization-specific response in *Ruegeria* MC10

To elucidate the functional response of *Ruegeria* MC10 to host-derived signals, we conducted comparative proteomic profiling of strains MC10-B4, MC0-A5, and MC15-BG7 following exposure to macerated coral tissue extract. Our analysis identified 6,267 expressed proteins across all conditions, with 5,528 high-confidence proteins retained after stringent filtering, clustered into 2,645 orthologous gene (OG) groups (Dataset S3). The proteomic response to host metabolites was substantial and comparable in scale across the three sympatric, coral-associated *Ruegeria* strains. Significant differential expression (FDR < 0.05, $|\log_2 FC| > 0.5$) was observed in 583/2222 (26%) OGs in MC10-B4 (Dataset S4), 773/1980 OGs (39%) in MC0-A5 (Dataset S5), and 522/1793 OGs (29%) in MC15-BG7 (Dataset S6). However, the direction of regulation differed markedly: MC0-A5 showed a strong bias toward upregulation (590 up vs. 183 down), whereas both MC10-B4 (191 up vs. 392 down) and MC15-BG7 (182 up vs. 340 down) were predominantly downregulated. Principal Coordinate Analysis (PCoA) revealed that bacterial strain identity was the primary driver of proteomic variation, explaining a significant proportion of the variance along PCoA1 (55.7%) and PCoA2 (37.75%) (Fig. 4A). Notably, the proteome of MC10-B4 was distinctly separated from those of MC0-A5 and MC15-BG7 along both axes, with the latter two strains separated from each other along PCoA2 but not PCoA1, underscoring the unique functional state of MC10-B4.

Exposure to coral tissue extract induced discernible shifts in the proteome of each strain, providing a dynamic view of their host interaction strategies. The response of MC10-B4 was particularly revealing. Upon exposure to host metabolites, MC10-B4 exhibited a significant downregulation of genes encoding machinery for active dispersal and adhesion (Pizarro-Cerdá et al., 2006; Shi et al., 2002), including Tad pilus assembly components (*tadB*, *tadG*), a VirB11-like conjugation/secretion system ATPase (*virB11*), flagellar motor torque generators (*motB*), and the flagellar structural protein (*fliL*) (Fig. 4B). Conversely, MC10-B4 upregulated the flagellar filament protein (*fliC*) and the MS-ring component (*fliF*). This pattern suggests strategic reprogramming where energy is diverted away from active motility and adhesion structures, while potentially maintaining a basal flagellar apparatus. Notably, its enhanced biofilm-forming capacity, observed in phenotypic assays, was not associated with the upregulation of its unique GT or EPS biosynthesis genes. Among those detected in the proteome, a GT2 family and a GT51 family were downregulated while another GT2 family, *exoP*, and *exoU* showed no significant change, suggesting this trait is a constitutive property based on its genomic endowment rather than a metabolically induced response during initial host encounter. Concurrently, MC10-B4 exhibited a coordinated upregulation of pathways associated with a sessile lifestyle, including the acyl-homoserine lactone (AHL) synthase *lasI* (quorum sensing), the phosphonate metabolism gene *phnA* (nutrient scavenging and quorum sensing regulator) (Choi et al., 2011; Jones et al., 2022), and adenylate cyclase *acyC*/*cyaB* (cAMP signaling potentially for biofilm formation). This concerted response is consistent

with a metabolic shift where MC10-B4 initiates a transition from a motile, free-living state to a sessile, host-attached state conducive to stable colonization. In contrast, MC0-A5 robustly upregulated a broader suite of motility and adhesion genes (*cpaBCE*, *tadB*, *tadC*, *tadG*, *flgEHI*, *fliL*, *motA*), while MC15-BG7 displayed a mixed profile, significantly upregulating *fliC* but downregulating *virB11* and *tadG*.

Beyond motility and biofilm, coral tissue extract induced widespread metabolic reprogramming, revealing starkly different responses between MC10-B4 and the control strains. Analysis of nitrogen metabolism revealed that MC10-B4 markedly downregulated the energetically costly denitrification pathway (*narG*, *narJ*, *narK*, *norC*) while selectively upregulating the nitrite reductase *nirS*, resulting in a proteomic profile inconsistent with complete denitrification. In contrast, MC0-A5 upregulated genes for anaerobic respiration (*napA*, *napC*, *norZ*), while MC15-BG7, which genomically lacks this machinery, showed no detectable expression of these pathways. A divergent pattern emerged in DMSP processing, where MC10-B4 downregulated the demethylation genes *dmdA* and *dmdB*, suggesting a reduced catabolism of this host-derived antioxidant. Conversely, MC0-A5 upregulated other DMSP catabolism genes (*dmdB*, *dmdC*), though the absence of a detectable *dmdA* suggests an alternative functional context (Reisch et al., 2011). Strikingly, vitamin B_{12} biosynthesis showed a paradoxical activation in MC10-B4; despite carrying several pseudogenes in the pathway, the strain expressed the full suite of biosynthetic proteins, whereas the control strains MC0-A5 and MC15-BG7, with genomically complete pathways, did not express several of the corresponding proteins. This collective reprogramming in MC10-B4, characterized by the strategic suppression of some pathways and the specific activation of others, is consistent with a substantial reallocation of cellular resources for host integration.

Discussion

The accelerating decline of coral reefs demands innovative and scalable interventions. We recently proposed an evolution-guided framework to overcome a key bottleneck in probiotic application, namely the uncertain long-term colonization of administered microbes, by selecting candidates based on genomic signatures of host dependency (Xie et al., 2025). The *Ruegeria* MC10 strain B4, identified through this framework, subsequently demonstrated sustained retention and association with increased thermal resilience in corals (Xie et al., 2025). The current study uses integrated multi-omics to investigate the potential mechanisms underlying long-term host association and host benefit. Our *ex hospite* analyses lend mechanistic support to the hypothesis that MC10's genomic architecture is linked to a functional state consistent with persistent host colonization. This approach suggests that targeting an evolutionary trajectory toward host dependency could help pre-select for probiotics with a high *a priori* potential for stable colonization.

Our genomic analysis indicates that *Ruegeria* MC10 possesses a distinct architecture indicative of a host-adapted lifestyle at an early stage of symbiotic integration. A recent model by Siozios et al. (Siozios et al., 2024) posits that the initial transition to endosymbiosis is characterized by a phase of genome expansion, driven by the loss of CRISPR-Cas defenses and a consequent proliferation of mobile genetic elements (MGEs) that provide novel adaptive traits, such as effectors for host interaction. In line with this model, *Ruegeria* MC10 exhibits a larger chromosome size, enriched with insertion sequences, prophages, and

integrated plasmids, consistent with its recent adoption of a host-dependent lifestyle. However, MC10 presents a fascinating nuance: unlike the *Arsenophonus* symbionts described by Siozios et al., it has acquired and maintained a diverse arsenal of defense systems, including restriction-modification systems, toxin-antitoxin modules, and Cas genes, which are largely absent from its sister populations. This suggests that the evolutionary path to host dependency may not universally require the complete disarmament of genomic defenses. Instead, MC10 may represent a state where the benefits of certain MGEs are harnessed while core defensive capabilities are actively gained, potentially for stability in a still-competitive environment or to regulate the very MGEs that facilitate adaptation. Thus, while MC10's genome expansion firmly places it in the early, innovative phase of symbiotic transition outlined by Siozios et al., its uniquely acquired defense repertoire highlights an alternative, and potentially more stable, trajectory within this model. Critically, comparative analysis revealed that alongside its metabolic decay, MC10 has acquired a unique genetic repertoire. This repertoire includes genes coding for traits such as a complete siderophore system, which is absent in its closest relatives and could provide a high-affinity mechanism for scavenging iron in the host's typically iron-limited environment. This is complemented by a specialized oxidative stress defense system, theoretically advantageous for persistence within the microoxic and immune-reactive milieu of the host gastrodermis. Thus, the MC10 genome appears to be characterized by a combination of reductive and acquisitive evolution, a pattern consistent with an early transition towards host association where the benefits of new functional traits for host interaction are selected for.

The phenotypic traits of MC10-B4, observed *in vitro*, provide evidence for functional realization of its genomic predictions and are suggestive of a host-adapted state. The production of siderophore and its capacity for robust biofilm formation align with the presence of its distinct genetic clusters for siderophore production and extracellular matrix components. While a direct genotype-phenotype link would require further genetic validation, the confirmed traits can arguably be advantageous for establishing residency in a host environment. Notably, the expression of its unique glycosyltransferase and EPS genes was constitutive and not upregulated by host metabolites, in contrast to the induced expression of similar genes in the coral symbiont *Endozoicomonas marisrubri* (Pogoreutz et al., 2022). This suggests MC10 may employ a distinct strategy for host association, relying on a pre-formed capacity for attachment rather than a host-cue-induced investment. Collectively, this host-adapted strategy aligns with a profile of constrained independent fitness, evidenced by the observed sensitivity to H_2O_2 and the inherent metabolic inefficiencies suggested by MC10's genomic decay, which paint a picture of a bacterium that is not a robust free-living competitor. This collective phenotypic profile, including a general susceptibility to various stressors under laboratory conditions, aligns with the evolutionary trajectory predicted by its genomic signatures of host dependency and is consistent with a lifestyle oriented toward a host-associated niche.

The proteomic response to host metabolites offers a dynamic, yet still *ex hospite*, view of how MC10-B4 might initiate colonization. Exposure to coral tissue extract triggered a significant downregulation of motility and adhesion machinery (e.g., Tad pilus components, flagellar motors) alongside a concurrent upregulation of pathways associated with a sessile lifestyle, including quorum sensing and cAMP signaling. This concerted "motility-to-sessility"

shift, supported by the observed capacity for biofilm formation, is consistent with the initiation of a stable, host-attached state. The response also included a notable metabolic reprogramming, where MC10-B4 downregulated energetically costly pathways like full-scale denitrification, yet selectively upregulated the nitrite reductase *nirS*. The specific upregulation of *nirS*, an enzyme that produces nitric oxide (NO), is particularly intriguing. In beneficial symbioses, NO is increasingly recognized not merely as a toxin but as a pluripotent signaling molecule that can modulate host-microbe interactions, for instance by preparing symbionts for oxidative stress and contributing to colonization specificity (Wang and Ruby, 2011). Furthermore, the observed downregulation of the DMSP demethylation genes (*dmdA*, *dmdB*) is noteworthy. The *dmdA*-mediated pathway, often screened for in conventional probiotics (Santoro et al., 2021), directs the antioxidant DMSP (Sunda et al., 2002) towards bacterial sulfur assimilation. Its downregulation suggests that MC10-B4 may minimize its catabolism of this coral holobiont-derived antioxidant. This could potentially function to preserve DMSP and its derivatives for holobiont-level oxidative stress protection, representing a putative host-beneficial trait that aligns with its evolutionarily selected role as a stable symbiont.

The functional profile of *Ruegeria* MC10 stands in stark contrast to the traits typically selected for in conventional probiotic screens. Traditional approaches often prioritize bacterial performance *in vitro*, operating on the assumption that traits like high antioxidant activity or rapid nutrient cycling will function similarly within the host environment. For instance, resistance to oxidative stress is a common selection criterion (Dungan et al., 2022; Santoro et al., 2021), based on the premise that probiotics could mitigate host bleaching. Counter to this, MC10-B4 is uniquely sensitive to H_2O_2, a trait consistent with potential avoidance of the high-ROS symbiosome niche. Similarly, while the presence of genes like the DMSP demethylase *dmdA* is used as a proxy for a beneficial function (Santoro et al., 2021), MC10-B4 downregulated this pathway upon host exposure, suggesting a catabolic strategy that may preserve holobiont DMSP antioxidants. Therefore, the very traits that would have excluded MC10 from conventional screens are likely integral to its successful host adaptation, validating an evolution-guided approach that selects for innate colonization potential over pre-defined *in vitro* functionalities.

For a symbiont to achieve long-term residency, it must navigate the dual challenges of host-derived stress and competition from other microbes. Our *ex hospite* analyses suggest MC10 employs a strategy of niche specialization complemented by genomic resilience. Phenotypically, MC10-B4's sensitivity to H_2O_2 and low pH indicates an avoidance of the most hostile microenvironments, such as the direct vicinity of Symbiodiniaceae, a finding consistent with our FISH imaging (Xie et al., 2025). Instead, it likely occupies a more buffered niche within the host. Genomically, this is supported by features such as a complete Class Ib ribonucleotide reductase (RNR) operon, which supports DNA repair and maintenance of dNTP pools under oxidative stress. Furthermore, the arsenal of defense systems uniquely acquired by MC10, including toxin-antitoxin modules, Cas genes, and restriction-modification systems, may provide a crucial line of defense against genomic parasites like phages. While their efficacy *in hospite* requires validation, the presence of these systems suggests an evolutionary investment in genomic stability. This combination of niche selection and genomic defense mechanisms could be key to mitigating the inherent costs of

its metabolic dependencies, thereby facilitating not just initial colonization but also sustained persistence.

Collectively, our *ex hospite* multi-omics data support a model where *Ruegeria* MC10's evolutionary trajectory toward host dependency is functionally underpinned by a suite of traits conducive to stable colonization. This includes a unique genomic repertoire for stress management and a phenotypic profile marked by robust biofilm formation alongside metabolic constraints, such as impaired growth (Xie et al., 2025) and stress susceptibility, that are consistent with its genomic decay. This propensity for a sessile lifestyle is further supported by the proteomic response to host metabolites, which revealed a "motility-to-sessility" shift characterized by the downregulation of motility genes. This proposed behavioral shift finds a compelling parallel in the coral symbiont *Endozoicomonas marisrubri*, which also downregulates flagellar genes upon host exposure (Pogoreutz et al., 2022), suggesting a convergent strategy for colonization initiation. While direct *in hospite* validation is a critical next step, this work demonstrates how an evolution-guided framework, which initially identifies candidates based on genomic signatures of host dependency (e.g., insertion sequence expansion and pseudogene proliferation), can subsequently uncover the functional traits and mechanistic hypotheses that may explain their probiotic efficacy. The principle of selecting for stability to increase the predictive power in identifying probiotics capable of long-term colonization holds potential for application beyond coral reefs, offering a generalizable strategy for microbiome engineering in conservation, aquaculture, and agriculture where durable host-microbe relationships are a shared goal.

Acknowledgements: We would like to thank Xiao Chu and Yanfeng Xing for their contributions on compiling and curating metabolism-related genes. We would like to thank Xiaojun Wang and Wudi Gai for suggestions on bioinformatics. We would like to thank Yumei Chen, Zhihao Xian, Jeremy Ho, and Kai Yan Lai for their support in phenotypic and morphological experiments.

Funding: This study is supported by Hong Kong Research Grants Council (RGC) General Research Fund (project #: 14114724), along with a Direct Grant from CUHK Faculty of Science (project #: 4053691), granted to H.L. C.P. was supported by an ANR Junior Professor Grant 'A connected underwater world' ANR-22-CPJ2-0113-01 awarded by the French National Research Agency (ANR). C.R.V. acknowledges funding from the German Research Foundation (DFG) project no. 458901010.

Data availability: Raw genome sequencing data are available on NCBI under several BioProjects with the private access link for reviewers. The raw reads of 409 and assembled genomes of 419 *Ruegeria* isolates (10 genomes missing raw data) sequenced on the second-generation platform (DNBseq) and 34 *Ruegeria* isolates sequenced on the third-generation platform (Nanopore) are available under NCBI BioProject accessions PRJNA1264799 (https://dataview.ncbi.nlm.nih.gov/object/PRJNA1264799?reviewer=mp7rulknapinfb95c9733nf72r) and PRJNA1275854 (https://dataview.ncbi.nlm.nih.gov/object/PRJNA1275854?reviewer=g4mffnb8b965tq6b2662cpt6i8), respectively. The mass spectrometry output files have been deposited in the

ProteomeXchange Consortium via the PRIDE partner repository with the dataset identifier PXD069552.

References

Abby, S. S., Néron, B., Ménager, H., Touchon, M., & Rocha, E. P. (2014). MacSyFinder: a program to mine genomes for molecular systems with an application to CRISPR-Cas systems. *PLoS One, 9*(10), e110726.

Barott, K. L., Venn, A. A., Perez, S. O., Tambutté, S., & Tresguerres, M. (2015). Coral host cells acidify symbiotic algal microenvironment to promote photosynthesis. *Proceedings of the National Academy of Sciences, 112*(2), 607-612.

Barrangou, R., & Marraffini, L. A. (2014). CRISPR-Cas systems: prokaryotes upgrade to adaptive immunity. *Molecular cell, 54*(2), 234-244.

Blin, K., Shaw, S., Augustijn, H. E., Reitz, Z. L., Biermann, F., Alanjary, M., et al. (2023). antiSMASH 7.0: new and improved predictions for detection, regulation, chemical structures and visualisation. *Nucleic acids research, 51*(W1), W46-W50.

Cai, Y., Jaecklein, E., Mackenzie, J. S., Papavinasasundaram, K., Olive, A. J., Chen, X., et al. (2021). Host immunity increases Mycobacterium tuberculosis reliance on cytochrome bd oxidase. *PLoS Pathogens, 17*(7), e1008911.

Čaušević, S., Dubey, M., Morales, M., Salazar, G., Sentchilo, V., Carraro, N., et al. (2024). Niche availability and competitive loss by facilitation control proliferation of bacterial strains intended for soil microbiome interventions. *Nature communications, 15*(1), 2557.

Choi, Y., Park, H.-Y., Park, S. J., Park, S.-J., Kim, S.-K., Ha, C., et al. (2011). Growth phase-differential quorum sensing regulation of anthranilate metabolism in Pseudomonas aeruginosa. *Molecules and cells, 32*(1), 57-65.

Clay, K. (2014). Defensive symbiosis: a microbial perspective. *Functional Ecology, 28*(2), 293-298.

Dellisanti, W., Zhang, Q., Ferrier-Pagès, C., & Kühl, M. (2024). Contrasting effects of increasing dissolved iron on photosynthesis and O2 availability in the gastric cavity of two Mediterranean corals. *PeerJ, 12*, e17259.

Dörr, M., Denger, J., Maier, C. S., Kirsch, J. V., Manns, H., & Voolstra, C. R. (2023). Short-term heat stress assays resolve effects of host strain, repeat stress, and bacterial inoculation on Aiptasia thermal tolerance phenotypes. *Coral Reefs, 42*(6), 1271-1281.

Dungan, A. M., Hartman, L. M., Blackall, L. L., & van Oppen, M. J. (2022). Exploring microbiome engineering as a strategy for improved thermal tolerance in Exaiptasia diaphana. *Journal of Applied Microbiology, 132*(4), 2940-2956.

Emms, D. M., & Kelly, S. (2015). OrthoFinder: solving fundamental biases in whole genome comparisons dramatically improves orthogroup inference accuracy. *Genome biology, 16*(1), 157.

Feng, Y., Wang, Z., Chien, K.-Y., Chen, H.-L., Liang, Y.-H., Hua, X., et al. (2022). “Pseudo-pseudogenes” in bacterial genomes: Proteogenomics reveals a wide but low protein expression of pseudogenes in Salmonella enterica. *Nucleic acids research, 50*(9), 5158-5170.

Ganesan, R., Wierz, J. C., Kaltenpoth, M., & Flórez, L. V. (2022). How it all begins: bacterial factors mediating the colonization of invertebrate hosts by beneficial symbionts. *Microbiology and Molecular Biology Reviews, 86*(4), e00126-00121.

Getz, L. J., & Maxwell, K. L. (2024). Diverse antiphage defenses are widespread among prophages and mobile genetic elements. *Annual Review of Virology, 11*.

Giuffrè, A., Borisov, V. B., Arese, M., Sarti, P., & Forte, E. (2014). Cytochrome bd oxidase and bacterial tolerance to oxidative and nitrosative stress. *Biochimica et Biophysica Acta (BBA)-Bioenergetics, 1837*(7), 1178-1187.

Hood, M. I., & Skaar, E. P. (2012). Nutritional immunity: transition metals at the pathogen–host interface. *Nature Reviews Microbiology, 10*(8), 525-537.

Hughes, T. P., Barnes, M. L., Bellwood, D. R., Cinner, J. E., Cumming, G. S., Jackson, J. B., et al. (2017). Coral reefs in the Anthropocene. *Nature, 546*(7656), 82-90.

Jones, C. J., Grotewold, N., Wozniak, D. J., & Gloag, E. S. (2022). Pseudomonas aeruginosa initiates a rapid and specific transcriptional response during surface attachment. *Journal of bacteriology, 204*(5), e00086-00022.

Lesser, M. P. (2006). Oxidative stress in marine environments: biochemistry and physiological ecology. *Annu. Rev. Physiol., 68*, 253-278.

Li, J., Zou, Y., Li, Q., Zhang, J., Bourne, D. G., Lyu, Y., et al. (2023). A coral-associated actinobacterium mitigates coral bleaching under heat stress. *Environmental Microbiome, 18*(1), 83.

Louden, B. C., Haarmann, D., & Lynne, A. M. (2011). Use of blue agar CAS assay for siderophore detection. *Journal of microbiology & biology education, 12*(1), 51-53.

Marquet, M., Hölzer, M., Pletz, M. W., Viehweger, A., Makarewicz, O., Ehricht, R., et al. (2022). What the Phage: a scalable workflow for the identification and analysis of phage sequences. *Gigascience, 11*, giac110.

Nadell, C. D., Drescher, K., Wingreen, N. S., & Bassler, B. L. (2015). Extracellular matrix structure governs invasion resistance in bacterial biofilms. *The ISME Journal, 9*(8), 1700-1709.

Orsburn, B. C. (2021). Proteome discoverer—a community enhanced data processing suite for protein informatics. *Proteomes, 9*(1), 15.

Peixoto, R. S., Sweet, M., Villela, H. D., Cardoso, P., Thomas, T., Voolstra, C. R., et al. (2021). Coral probiotics: premise, promise, prospects. *Annual review of animal biosciences, 9*(1), 265-288.

Pizarro-Cerdá, J., & Cossart, P. (2006). Bacterial adhesion and entry into host cells. *Cell, 124*(4), 715-727.

Pogoreutz, C., Oakley, C. A., Rädecker, N., Cárdenas, A., Perna, G., Xiang, N., et al. (2022). Coral holobiont cues prime Endozoicomonas for a symbiotic lifestyle. *The ISME Journal, 16*(8), 1883-1895.

Rädecker, N., Pogoreutz, C., Gegner, H. M., Cárdenas, A., Roth, F., Bougoure, J., et al. (2021). Heat stress destabilizes symbiotic nutrient cycling in corals. *Proceedings of the National Academy of Sciences, 118*(5), e2022653118.

Ravichandran, S., Thangarasu, D., Ravichandran, A., Dorai, S., Ayyadurai, N., Sivapackiam, J., et al. (2025). Coral Microbiomes and Biofilms: Ecological Features, Response to Microbial Infections, and Conservation Strategies. *Marine Ecology, 46*(4), e70036.

Reimer, J. D., Peixoto, R. S., Davies, S. W., Traylor-Knowles, N., Short, M. L., Cabral-Tena, R. A., et al. (2024). The fourth global coral bleaching event: where do we go from here? *Coral Reefs, 43*(4), 1121-1125.

Reisch, C. R., Stoudemayer, M. J., Varaljay, V. A., Amster, I. J., Moran, M. A., & Whitman, W. B. (2011). Novel pathway for assimilation of dimethylsulphoniopropionate widespread in marine bacteria. *Nature, 473*(7346), 208-211.

Roca, I., Torrents, E., Sahlin, M., Gibert, I., & Sjo□berg, B.-M. (2008). NrdI essentiality for class Ib ribonucleotide reduction in Streptococcus pyogenes. *Journal of bacteriology, 190*(14), 4849-4858.

Santoro, E. P., Borges, R. M., Espinoza, J. L., Freire, M., Messias, C. S., Villela, H. D., et al. (2021). Coral microbiome manipulation elicits metabolic and genetic restructuring to mitigate heat stress and evade mortality. *Science Advances, 7*(33), eabg3088.

Sedlacek, P., Slaninova, E., Koller, M., Nebesarova, J., Marova, I., Krzyzanek, V., et al. (2019). PHA granules help bacterial cells to preserve cell integrity when exposed to sudden osmotic imbalances. *New biotechnology, 49*, 129-136.

Shi, W., & Sun, H. (2002). Type IV pilus-dependent motility and its possible role in bacterial pathogenesis. *Infection and Immunity, 70*(1), 1-4.

Siozios, S., Nadal-Jimenez, P., Azagi, T., Sprong, H., Frost, C. L., Parratt, S. R., et al. (2024). Genome dynamics across the evolutionary transition to endosymbiosis. *Current Biology, 34*(24), 5659-5670. e5657.

Skorupska, A., Janczarek, M., Marczak, M., Mazur, A., & Król, J. (2006). Rhizobial exopolysaccharides: genetic control and symbiotic functions. *Microbial cell factories, 5*, 1-19.

Sunda, W., Kieber, D., Kiene, R., & Huntsman, S. (2002). An antioxidant function for DMSP and DMS in marine algae. *Nature, 418*(6895), 317-320.

Voolstra, C. R., Suggett, D. J., Peixoto, R. S., Parkinson, J. E., Quigley, K. M., Silveira, C. B., et al. (2021). Extending the natural adaptive capacity of coral holobionts. *Nature Reviews Earth & Environment, 2*(11), 747-762.

Wishart, D. S., Han, S., Saha, S., Oler, E., Peters, H., Grant, J. R., et al. (2023). PHASTEST: faster than PHASTER, better than PHAST. *Nucleic acids research, 51*(W1), W443-W450.

Xie, M., Xiang, N., Liao, T., Cheung, C. T., Lee, C. H., Tse, W. Y., et al. (2025). Evolutionary Genomics Guides Scalable Coral Probiotics for Climate Resilience. *BioRxiv*, 2025.2006. 2016.659728.

Xue, C.-X., Lin, H., Zhu, X.-Y., Liu, J., Zhang, Y., Rowley, G., et al. (2021). DiTing: a pipeline to infer and compare biogeochemical pathways from metagenomic and metatranscriptomic data. *Frontiers in microbiology, 12*, 698286.

Legends of figures

Fig. 1. Comparative genomic analysis of the 35 *Ruegeria* strains. (**A**) Upper: Presence/absence patterns of orthologous gene (OG) groups in plasmids and chromosomes, clustered by strain-specific gene content variations. Three annotation columns indicate metadata of *Ruegeria* isolates (coral species, sampling site, coral compartment). Gene status (pseudogene vs. intact gene) is color-coded by genomic location (plasmid/chromosome). The integrated chromosomal sequences in MC10 homologous to plasmids in other MCs was shown in a dashed frame. Lower: Scatter plot showing OG distribution across *Ruegeria* populations. Each OG is represented by a single point. Red points (Global persistence) show the percentage of all 35 genomes that contain a given OG, calculated as (number of genomes containing the OG)/(total 35 genomes). Blue points (MC10-specific relative persistence) show a normalized measure of how concentrated an OG is within the MC10 population, calculated as (number of MC10 strains containing the OG)/(number of genomes containing the OG). Colored outlines highlight key distributions: yellow for OGs sparsely distributed in other MCs, purple for OGs conserved in all populations, and red for OGs uniquely prevalent in the MC10 population. (**B**) Stacked bar plot comparing chromosomal and plasmid sizes across strains based on Canu assemblies (~4.5 Mb). MC10-D9 and MC10-B7 show nearly closed genomes (two contigs: the larger chromosome and a smaller contig labeled Chr_contig2), MC10-AC11 has a less complete assembly (~3.51 Mb), while other MC10 members possess complete single-chromosome assemblies. (**C**) Stacked bar plot showing the distribution of integrated prophage lengths across strains, with each colored segment representing an individual prophage region (Prophages 1 to 5).

Fig. 2. Functional gene distribution across the 35 closed *Ruegeria* genomes. (**A**) The heatmap depicts the presence and absence patterns of MC10-enriched genes associated with key adaptive traits including oxidative stress response, siderophore production, toxin-antitoxin system, and Cas genes. (**B**) Glycosyltransferase (GT) family and extracellular polysaccharide (EPS) production-related gene distribution.

Fig. 3 Morphological and functional characterization of four *Ruegeria* strains.

(**A**) Transmission electron microscopy (TEM) images of *Ruegeria* type strain *R. pomeroyi* DSS-3, MC10-B4, MC0-A5, and MC15-BG7. Bright white granules correspond to intracellular storage inclusions, like starch and/or polyhydroxybutyrate (PHB), whereas light grey regions correspond to putative lipid droplets. Scale bars = 600 nm. (**B**) Bacterial swimming motility assay. (Top left panel) Representative images of swimming halos on 0.18% semi-solid marine broth 2216 agar plates after 6 days of incubation at 28 °C. Bacterial suspensions (5 μL) at logarithmic growth phase (OD_{600}=0.5) were point-inoculated at the centre of each plate. (Top right panel) Quantification of swimming motility, presented as the diameter of the halo. Data are shown as mean ± SD from three independent experiments: ns, not significant, ***, $P < 0.001$. (Bottom panel) Sedimentation phenotypes of the four strains after 24 h and 48 h of incubation at room temperature without shaking. DSS-3 and MC15-BG7 show a clear sedimentation phenotype, whereas MC10-B4 and MC0-A5 did not settle under the same conditions. (**C**) Swarming and twitching motility assays. (Top panel) Bacterial suspensions (5 μL) of four strains at logarithmic growth phase (OD_{600}=0.5) were spotted onto swarming plates (0.75% agar). (Bottom panel) For twitching motility, 1 μL of bacterial suspension was stab-inoculated into 1% agar plates. All plates were incubated at 28 °C for 10 days. To visualize twitching motility, the agar was carefully removed, and the adherent cells at the inoculation point were air-dried, fixed, and stained with 0.1% crystal violet. Images shown are from one experiment representative of three independent biological replicates. (**D**) Biofilm formation by four *Ruegeria* strains was quantified using crystal violet staining. After incubation in marine broth 2216 within a 96-well plate for 24 or 48 hours at 28 °C, the biofilm was stained with 0.1% crystal violet and subsequently decolorized with 0.2 ml decolorizing solution; absorbance was measured at OD_{590}. All test strains were grown on the same plate. Data represent the mean of six biological replicates, with error bars indicating standard deviations. MB: Marine broth medium 2216. ****, $P < 0.0001$. (**E**) Chrome azurol S (CAS) assay assessing siderophore production in the four *Ruegeria* strains. The red arrows point to the areas where the color changes from blue to yellow. (**F**) Growth of four *Ruegeria* strains assessed in marine basal medium (MBM) under different vitamin supplementation conditions. Four treatments were tested: (i) complete vitamin

supplementation, (ii) no vitamins, (iii) absence of vitamin B_7, and (iv) absence of vitamin B_{12}. Cultures were inoculated at an initial OD_{600} of 0.01 and incubated at 28 °C with shaking. Growth was monitored by measuring OD_{600} over time. Data represent the mean of three replicates, and error bars indicate standard deviations. (**G**) Ten-fold serial dilutions of the four strains were spotted onto marine broth 2216 agar plates containing the indicated concentrations of H_2O_2 (0, 0.05, 0.1 mM). Plates were imaged after 3 days of incubation. The bottom panel quantifies the bacterial counts (Colony Forming Units, CFU) under each condition. Data are presented as the mean ± SD from three independent biological replicates. ns, not significant; **, $P < 0.01$.

Fig. 4. Proteomic analysis of coral tissue extracts effects on *Ruegeria* MC10-B4 and its ecological counterparts MC0-A5 and MC15-BG7. (**A**) Principal Coordinate Analysis (PCoA; Bray-Curtis dissimilarity) reveals distinct protein expression profiles, with MC10-B4 separating from MC0-A5 and MC15-BG7 along both PCoA axes (PCoA1 and PCoA2), while MC0-A5 and MC15-BG7 differ only along PCoA2. Treatment groups (coral tissue extract-treated vs. untreated) are indicated by shapes. (**B**) Volcano plot of differential gene expression. Each point represents a single gene, plotted by its $\log_2$ fold-change ($\log_2$FC) and -$\log_{10}$(P-value). Genes are coloured based on differential expression status: red for significantly upregulated ($P < 0.05$, $\log_2$FC > 0.5), blue for significantly downregulated (P < 0.05, $\log_2$FC < -0.5), and grey for non-significant features. Selected genes of interest are further classified by function: orange for motility, purple for biofilm formation, and dark for other functions. Point geometry denotes annotation status: circles (•) for genes with a functional annotation and crosses (×) for uncharacterized genes. The horizontal dash line indicates the *P*-value threshold ($P = 0.05$), and vertical dashed lines mark the fold-change thresholds (|log2FC| = 0.5).

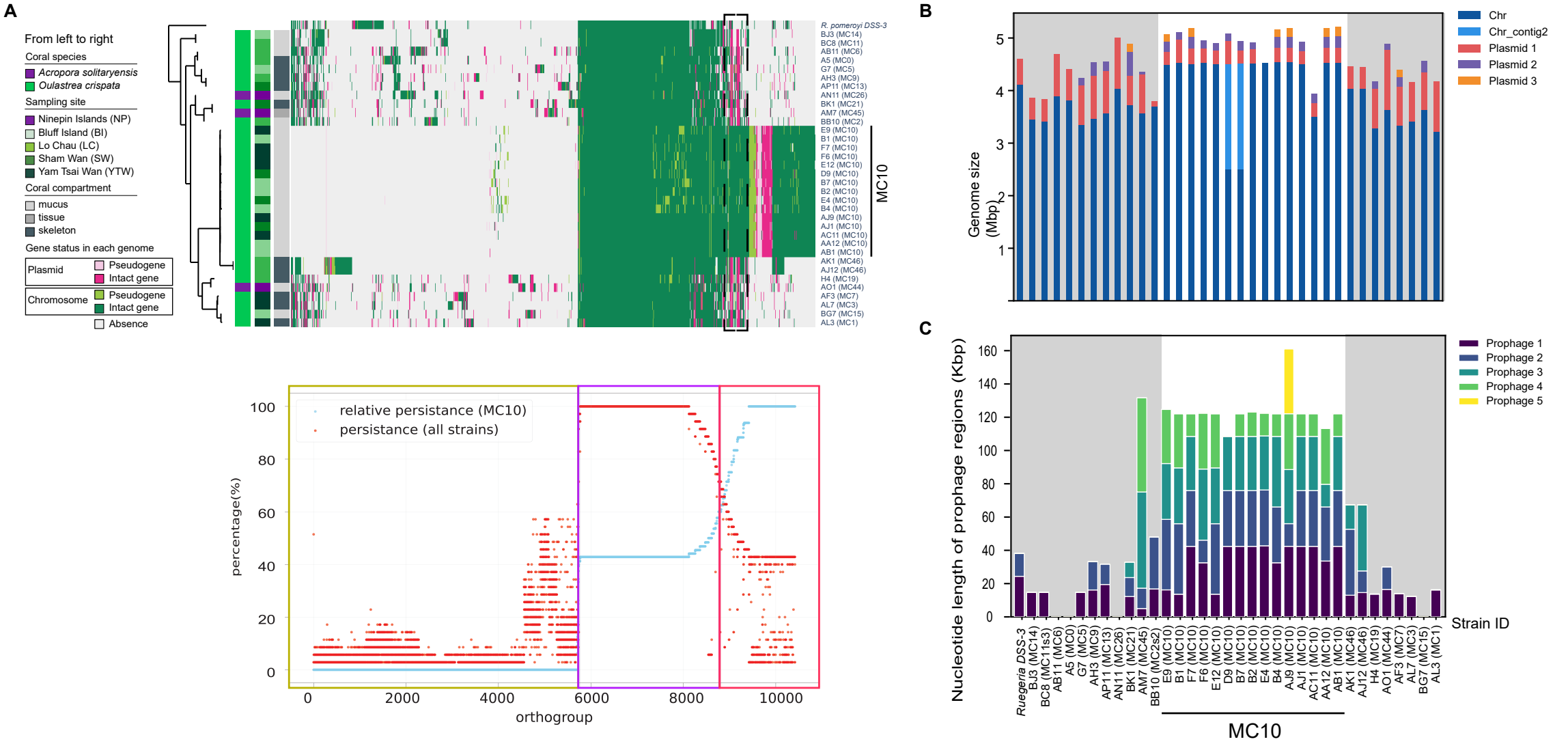
A
From left to right
Coral species
Acropora solitaryensis
Oulastrea crispata
Sampling site
Ninepin Islands (NP)
Bluff Island (BI)
Lo Chau (LC)
Sham Wan (SW)
Yam Tsai Wan (YTW)
Coral compartment
mucus
tissue
skeleton
Gene status in each genome
Plasmid
Pseudogene
Intact gene
Chromosome
Pseudogene
Intact gene
Absence
R. pomeroyi DSS-3
MC10
relative persistance (MC10)
persistance (all strains)
percentage(%)
orthogroup
B
Chr
Chr_contig2
Plasmid 1
Plasmid 2
Plasmid 3
Genome size (Mbp)
C
Prophage 1
Prophage 2
Prophage 3
Prophage 4
Prophage 5
Nucleotide length of prophage regions (Kbp)
Strain ID
Ruegeria DSS-3
MC10

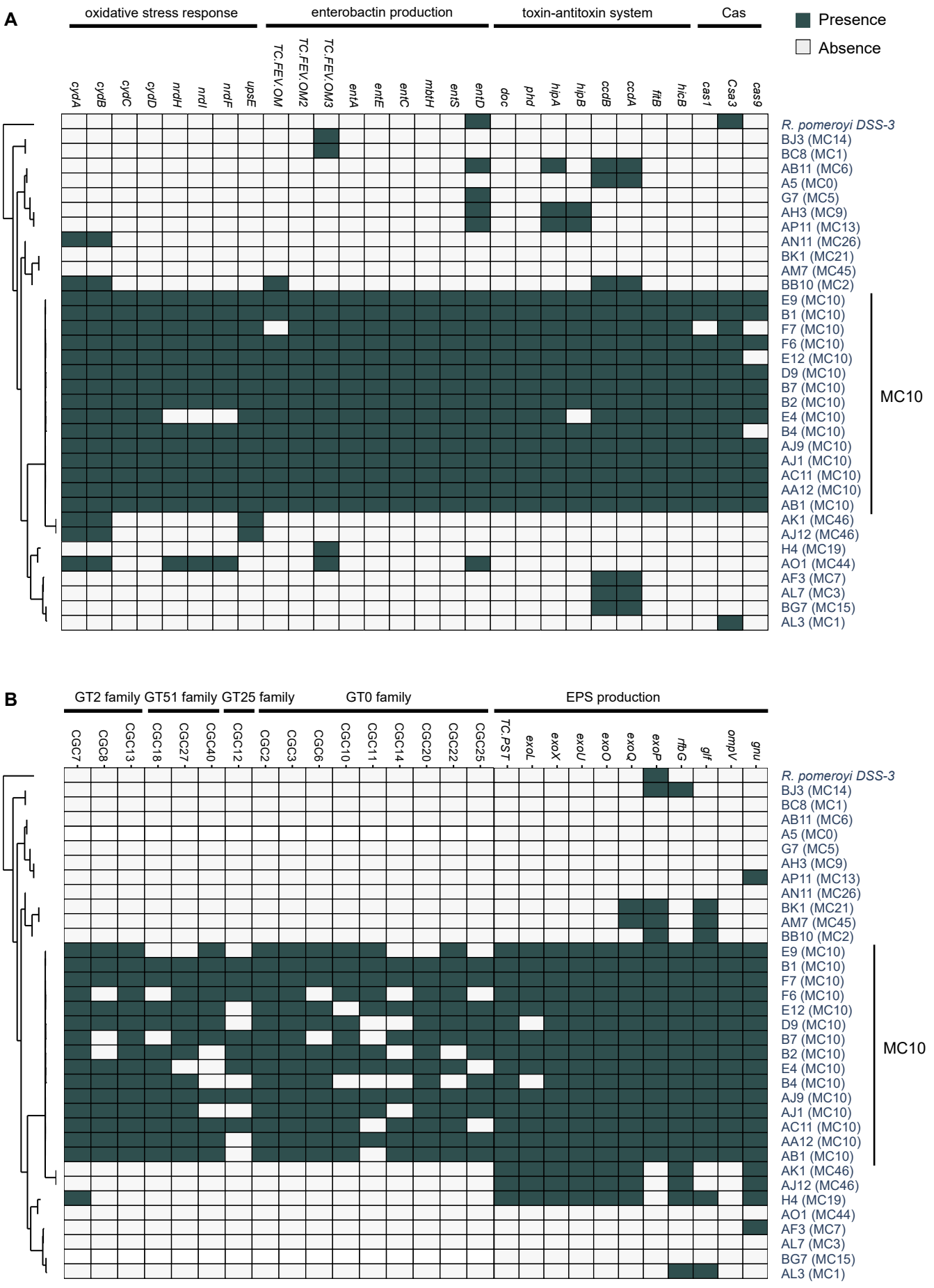
A
oxidative stress response
enterobactin production
toxin-antitoxin system
Cas
Presence
Absence
cydA
cydB
cydC
cydD
nrdH
nrdI
nrdF
upsE
TC.FEV.OM
TC.FEV.OM2
TC.FEV.OM3
entA
entE
entC
mbtH
entS
entD
doc
phd
hipA
hipB
ccdB
ccdA
fitB
hicB
cas1
Csa3
cas9
R. pomeroyi DSS-3
BJ3 (MC14)
BC8 (MC1)
AB11 (MC6)
A5 (MC0)
G7 (MC5)
AH3 (MC9)
AP11 (MC13)
AN11 (MC26)
BK1 (MC21)
AM7 (MC45)
BB10 (MC2)
E9 (MC10)
B1 (MC10)
F7 (MC10)
F6 (MC10)
E12 (MC10)
D9 (MC10)
B7 (MC10)
B2 (MC10)
E4 (MC10)
B4 (MC10)
AJ9 (MC10)
AJ1 (MC10)
AC11 (MC10)
AA12 (MC10)
AB1 (MC10)
MC10
AK1 (MC46)
AJ12 (MC46)
H4 (MC19)
AO1 (MC44)
AF3 (MC7)
AL7 (MC3)
BG7 (MC15)
AL3 (MC1)
B
GT2 family
GT51 family
GT25 family
GT0 family
EPS production
CGC7
CGC8
CGC13
CGC18
CGC27
CGC40
CGC12
CGC2
CGC3
CGC6
CGC10
CGC11
CGC14
CGC20
CGC22
CGC25
TC.PST
exoL
exoX
exoU
exoO
exoQ
exoP
rfbG
glf
ompV
gnu
R. pomeroyi DSS-3
BJ3 (MC14)
BC8 (MC1)
AB11 (MC6)
A5 (MC0)
G7 (MC5)
AH3 (MC9)
AP11 (MC13)
AN11 (MC26)
BK1 (MC21)
AM7 (MC45)
BB10 (MC2)
E9 (MC10)
B1 (MC10)
F7 (MC10)
F6 (MC10)
E12 (MC10)
D9 (MC10)
B7 (MC10)
B2 (MC10)
E4 (MC10)
B4 (MC10)
AJ9 (MC10)
AJ1 (MC10)
AC11 (MC10)
AA12 (MC10)
AB1 (MC10)
MC10
AK1 (MC46)
AJ12 (MC46)
H4 (MC19)
AO1 (MC44)
AF3 (MC7)
AL7 (MC3)
BG7 (MC15)
AL3 (MC1)

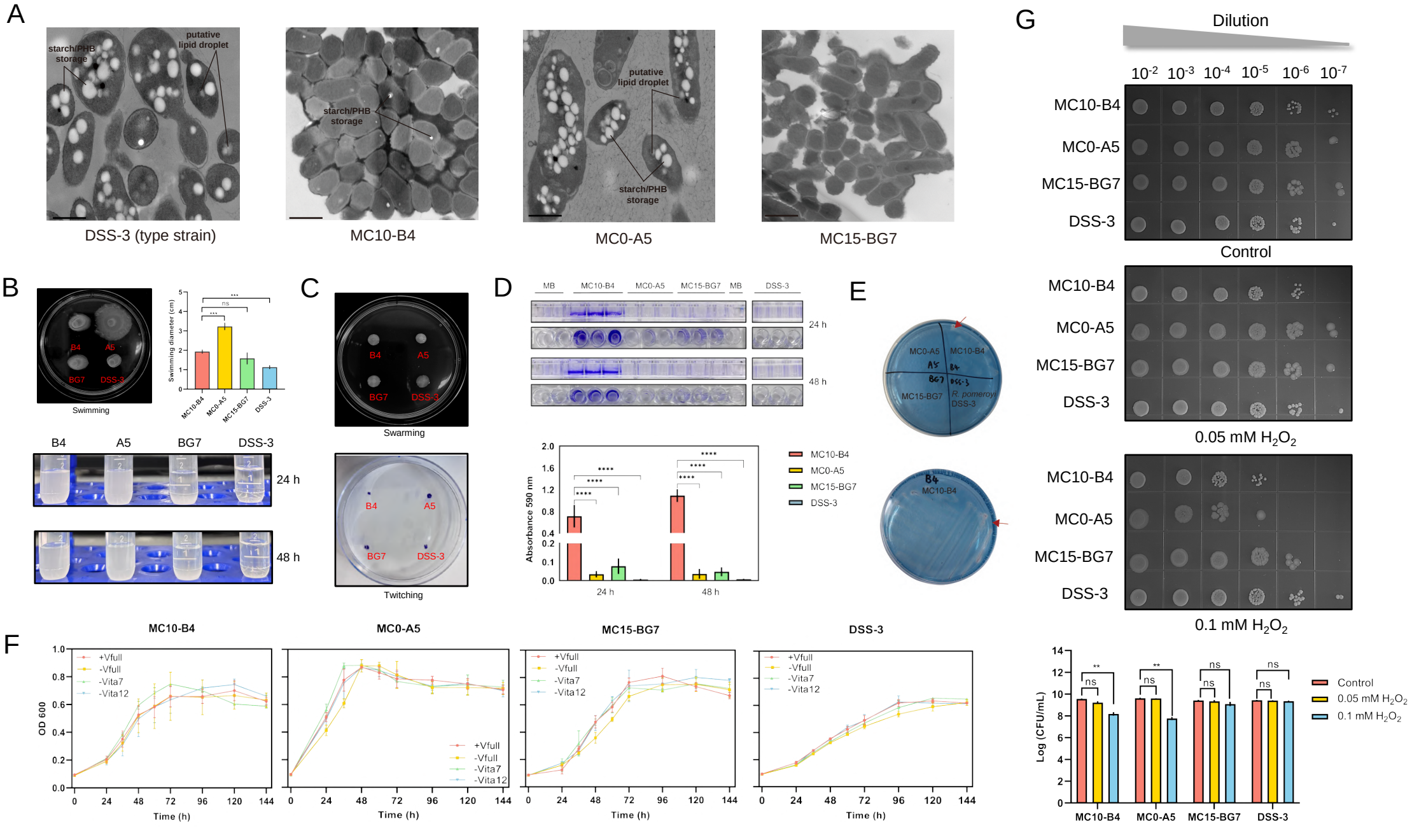
A
starch/PHB storage
putative lipid droplet
DSS-3 (type strain)
MC10-B4
MC0-A5
MC15-BG7
B
Swimming
Swimming diameter (cm)
MC10-B4
MC0-A5
MC15-BG7
DSS-3
B4
A5
BG7
DSS-3
24 h
48 h
C
Swarming
Twitching
D
MB
MC10-B4
MC0-A5
MC15-BG7
MB
DSS-3
24 h
48 h
Absorbance 590 nm
E
MC0-A5
MC10-B4
MC15-BG7
R. pomeroyi DSS-3
F
MC10-B4
MC0-A5
MC15-BG7
DSS-3
+Vfull
-Vfull
-Vita7
-Vita12
OD 600
Time (h)
G
Dilution
10-2 10-3 10-4 10-5 10-6 10-7
MC10-B4
MC0-A5
MC15-BG7
DSS-3
Control
0.05 mM H2O2
0.1 mM H2O2
Log (CFU/mL)
ns
Control
0.05 mM H2O2
0.1 mM H2O2

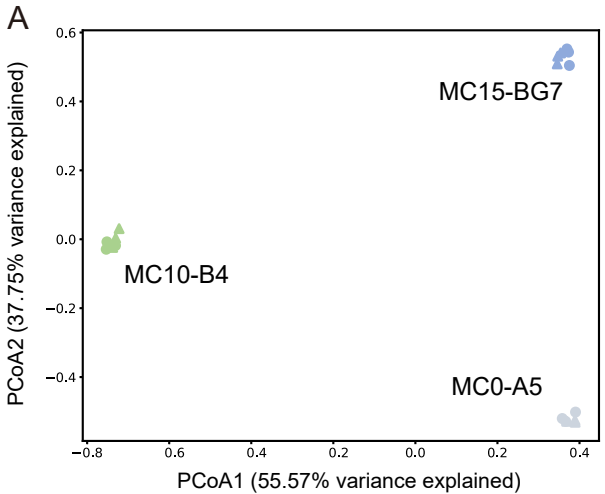
A
MC15-BG7
MC10-B4
MC0-A5
PCoA2 (37.75% variance explained)
PCoA1 (55.57% variance explained)
untreated group
coral tissue extract-treated group

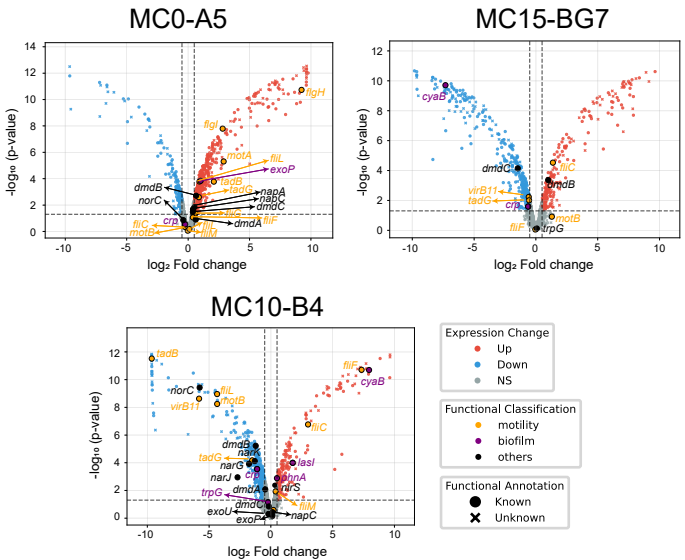
B
MC0-A5
MC15-BG7
MC10-B4
-log₁₀ (p-value)
log₂ Fold change
Expression Change
Up
Down
NS
Functional Classification
motility
biofilm
others
Functional Annotation
Known
Unknown